Electronic branching ratio of the τ lepton

R. Ammar,[a] P. Baringer,[a] D. Coppage,[a] R. Davis,[a] M. Kelly,[a] N. Kwak,[a]
H. Lam,[a] S. Ro,[a] Y. Kubota,[b] M. Lattery,[b] J. K. Nelson,[b] D. Perticone,[b] R. Poling,[b]
S. Schrenk,[b] R. Wang,[b] M. S. Alam,[c] I. J. Kim,[c] B. Nemati,[c] V. Romero,[c] C. R. Sun,[c]
P.-N. Wang,[c] M. M. Zoeller,[c] G. Crawford,[d] R. Fulton,[d] K. K. Gan,[d] H. Kagan,[d] R. Kass,[d]
J. Lee,[d] R. Malchow,[d] F. Morrow,[d] M. K. Sung,[d] J. Whitmore,[d] P. Wilson,[d] F. Butler,[e]
X. Fu,[e] G. Kalbfleisch,[e] M. Lambrecht,[e] P. Skubic,[e] J. Snow,[e] P.-L. Wang,[e] D. Bortoletto,[f]
D. N. Brown,[f] J. Dominick,[f] R. L. McIlwain,[f] D. H. Miller,[f] M. Modesitt,[f] E. I. Shibata,[f] S. F. Schaffner,[f]
I. P. J. Shipsey,[f] M. Battle,[g] J. Ernst,[g] H. Kroha,[g] S. Roberts,[g] K. Sparks,[g] E. H. Thorndike,[g]
C.-H. Wang,[g] R. Stroynowski,[h] M. Artuso,[i] M. Goldberg,[i] T. Haupt,[i] N. Horwitz,[i] R. Kennett,[i]
G. C. Moneti,[i] S. Playfer,[i] Y. Rozen,[i] P. Rubin,[i] T. Skwarnicki,[i] S. Stone,[i] M. Thulasidas,[i]
W.-M. Yao,[i] G. Zhu,[i] A. V. Barnes,[j] J. Bartelt,[j] S. E. Csorna,[j] V. Jain,[j] T. Letson,[j]
M. D. Mestayer,[j] D. S. Akerib,[k] B. Barish,[k] M. Chadha,[k] D. F. Cowen,[k] G. Eigen,[k] J. S. Miller,[k]
J. Urheim,[k] A. J. Weinstein,[k] R. J. Morrison,[l] H. Tajima,[l] D. Schmidt,[l] D. Sperka,[l] M. Procario,[m]
M. Daoudi,[n] W. T. Ford,[n] D. R. Johnson,[n] K. Lingel,[n] M. Lohner,[n] P. Rankin,[n] J. G. Smith,[n]
J. Alexander,[o] C. Bebek,[o] K. Berkelman,[o] D. Besson,[o] T. E. Browder,[o] D. G. Cassel,[o] E. Cheu,[o]
D. M. Coffman,[o] P. S. Drell,[o] R. Ehrlich,[o] R. S. Galik,[o] M. Garcia-Sciveres,[o] B. Geiser,[o] B. Gittelman,[o]
S. W. Gray,[o] D. L. Hartill,[o] B. K. Heltsley,[o] K. Honscheid,[o] C. Jones,[o] J. Kandaswamy,[o] N. Katayama,[o]
P. C. Kim,[o] D. L. Kreinick,[o] G. S. Ludwig,[o] J. Masui,[o] J. Mevissen,[o] N. B. Mistry,[o] S. Nandi,[o]
C. R. Ng,[o] E. Nordberg,[o] C. O'Grady,[o] J. R. Patterson,[o] D. Peterson,[o] D. Riley,[o] M. Sapper,[o]
M. Selen,[o] H. Worden,[o] M. Worris,[o] F. Würthwein,[o] P. Avery,[p] A. Freyberger,[p] J. Rodriguez,[p]
J. Yelton,[p] S. Henderson,[q] K. Kinoshita,[q] F. Pipkin,[q,*] M. Saulnier,[q] R. Wilson,[q] J. Wolinski,[q]
D. Xiao,[q] H. Yamamoto,[q] and A. J. Sadoff[r]

(CLEO Collaboration)

[a]*University of Kansas, Lawrence, Kansas 66045*
[b]*University of Minnesota, Minneapolis, Minnesota 55455*
[c]*State University of New York at Albany, Albany, New York 12222*
[d]*Ohio State University, Columbus, Ohio, 43210*
[e]*University of Oklahoma, Norman, Oklahoma 73019*
[f]*Purdue University, West Lafayette, Indiana 47907*
[g]*University of Rochester, Rochester, New York 14627*
[h]*Southern Methodist University, Dallas, Texas 75275*
[i]*Syracuse University, Syracuse, New York 13244*
[j]*Vanderbilt University, Nashville, Tennessee 37235*
[k]*California Institute of Technology, Pasadena, California 91125*
[l]*University of California at Santa Barbara, Santa Barbara, California 93106*
[m]*Carnegie-Mellon University, Pittsburgh, Pennsylvania, 15213*
[n]*University of Colorado, Boulder, Colorado 80309-0390*
[o]*Cornell University, Ithaca, New York 14853*
[p]*University of Florida, Gainesville, Florida 32611*
[q]*Harvard University, Cambridge, Massachusetts 02138*
[r]*Ithaca College, Ithaca, New York 14850*

(Received 2 December 1991)

Using data accumulated by the CLEO I detector operating at the Cornell Electron Storage Ring, we have measured the ratio $R=\Gamma(\tau\to e\bar{\nu}_e\nu_\tau)/\Gamma_1$, where Γ_1 is the τ decay rate to final states with one charged particle. We find $R=0.2231\pm0.0044\pm0.0073$ where the first error is statistical and the second is systematic. Together with the measured topological one-charged-particle branching fraction, this yields the branching fraction of the τ lepton to electrons, $B_e=0.192\pm0.004\pm0.006$.

PACS number(s): 13.35.+s, 14.60.Jj

I. INTRODUCTION

In the framework of the standard model of electroweak interactions, the τ is a sequential heavy lepton whose leptonic decays are well described by the theory. In particular, the standard model predicts the τ-decay width to an electron plus neutrino [1] and thereby relates the τ's electronic branching fraction B_e to its lifetime τ_τ:

$$\Gamma(\tau\to e\bar{\nu}_e\nu_\tau)=\frac{G_F^2 m_\tau^5}{192\hbar\pi^3}(1-\delta)=\frac{B_e}{\tau_\tau},$$

where m_τ and τ_τ are the τ mass and lifetime, respectively,

*Deceased.

G_F is the Fermi coupling constant, and δ is a QED correction. The current world averages [2] of the τ mass and lifetime are $m_\tau = 1784 \pm 3$ MeV/c^2 and $\tau_\tau = 0.303 \pm 0.008$ ps. These together with the value [2] of G_F, which has been precisely determined from muon decay, and the small QED correction [3] $\delta = 0.0042$, yield the expected electronic branching fraction of $B_e = 0.189 \pm 0.005$. This value differs by about two standard deviations from the current world average of the electronic branching fraction measurements [2]: $B_e = 0.177 \pm 0.004$. In this paper, we present a new measurement of the electronic branching fraction of the τ.

II. DATA SAMPLE AND METHOD

This analysis was based on data collected with the CLEO I detector operating at the Cornell Electron Storage Ring (CESR). At CESR τ pairs were produced in e^+e^- collisions with center-of-mass energies between 10.5 and 10.9 GeV. The data sample used in this analysis corresponded to an integrated luminosity of 429 pb^{-1}, or approximately 385 000 produced $\tau^+\tau^-$ pairs. The CLEO I detector is described in detail elsewhere [4]. Charged-particle tracking was accomplished with 64 layers of tracking in a 1.0-T magnetic field. The system achieved a momentum resolution of $(\delta p/p)^2 = (0.0023p)^2 + (0.007)^2$ where p is in GeV/c. Outside the solenoid, which encircled the central drift chamber, there were proportional chambers used to measure specific ionization (dE/dx), followed by time-of-flight counters and finally a lead/proportional tube electromagnetic calorimeter. These outer detectors were segmented into octants in azimuth. Electrons were identified using measurements of dE/dx, time of flight, and energy deposition in the time-of-flight counters and the calorimeter. In the 51 layer main drift chamber, the ionization loss was measured with a resolution of 6.5% and in the octant dE/dx modules, 124 measurements of specific ionization were made with a resolution of 6.0%. The time-of-flight system achieved a timing resolution of 350 ps rms including uncertainties in the beam crossing time. The electromagnetic calorimeters covered a solid angle of 47% of 4π and achieved an energy resolution $\sigma_E/E = 0.21/\sqrt{E}$ with E in GeV, and position resolution of 5 mm.

In order to measure the τ electronic branching ratio we first isolated events corresponding to $\tau^+\tau^-$ pair production. We used events in which one τ decayed to a final state with one charged particle and the other τ decayed to a final state with three charged particles. After subtracting backgrounds and correcting for efficiencies, we determined the fraction R of such "1-versus-3" decays in which the 1-prong track was an electron:

$$R = \frac{\Gamma(\tau \to e \bar{\nu}_e \nu_\tau)}{\Gamma_1} ,$$

where Γ_1 is the τ-decay rate to final states with one charged particle. This fraction was multiplied by the measured topological 1-prong branching ratio to obtain the branching fraction B_e.

The 1-versus-3 topology was used because for these events the trigger and reconstruction efficiency was high and could be modeled reliably. Using the ratio technique also reduced systematic uncertainties: many potential biases canceled, and the result was independent of the absolute integrated luminosity of the data sample. In order to avoid biasing the 1-prong decays, the selection criteria were applied primarily to the 3-prong side, and the same criteria were applied to all events.

At these center-of-mass energies a great deal of attention must be paid to the contamination of the τ data by non-τ decays. In addition to τ events, the selected four-track sample contained low-multiplicity hadronic final states, events of the type $e^+e^- \to e^+e^-X$, where X represents a lepton or quark pair ("two-photon" events), and events due to radiative Bhabha and muon pair production processes. In addition, it also contained events due to beam interactions with residual gas in the beam pipe ("beam-gas" events). We studied these backgrounds using Monte Carlo techniques and, whenever possible, the data themselves. In the Monte Carlo simulation, hadronic interactions, $e^+e^- \to q\bar{q}$, were generated using either Feynman-Field [5] with LUND 4.3 [6], or LUND 6.3 [7]. τ decays were produced using the KORALB event generator [8], and two-photon events were simulated using the prescription of Smith [9]. Generated events were then passed through a simulation of the CLEO I detector. Beam-gas events were studied by selecting events with charged particles originating far from the collision point along the beam axis.

III. EVENT SELECTION

We selected τ-pair candidate events by requiring exactly four charged particles with a net charge of zero. Each track had to be within the fiducial volume defined by $|\cos\theta| < 0.9$, where θ is the angle between the track and the electron beam direction, and had to pass within 5.0 mm of the beam axis. We then defined a 1-versus-3 prong topology by requiring that three of the charged particles in the event were separated from the fourth by more than 90°. If more than one track combination per event satisfied this condition, we chose the combination for which the angle between the lone track and the vector sum of the other three tracks was greatest. Events used in the analysis satisfied a trigger requiring at least three tracks and hits in nonadjacent octants of the time-of-flight counter. To minimize uncertainties in the trigger efficiency, we required one of the 3-prong tracks to point into the time-of-flight system by insisting $|\cos\theta| < 0.60$, while the 1-prong track had to lie within the more restricted fiducial volume defined by the electromagnetic calorimeter. In order to suppress beam-gas events, the event vertex had to lie within ± 5 cm of the nominal collision point along the beam axis. To suppress QED and hadronic backgrounds, events with an identified electron, muon, or kaon on the 3-prong side were eliminated. Photon conversions were suppressed by requiring that the invariant mass of all oppositely charged pairs of tracks, when assumed to be electrons, was greater than 100 Mev/c^2. Events with an identified secondary vertex due, for example, to photon conversion or K_S decay, were el-

iminated. Finally, in order to ensure reliable electron identification, the momentum of the lone track was required to be between 0.7 and 4.0 GeV/c. We note that only information on charged particles was used in the event selection; no requirements were made on neutral particles. Approximately 23 000 events satisfied these criteria.

Two-photon events tended to have low visible energy as shown in Fig. 1, and small net transverse momentum $|P_\perp|$, since these interactions generally had low center-of-mass energies and were boosted along the beam axis. To suppress these backgrounds we rejected events with a net $P_\perp^2$ less than 0.05 $(\mathrm{GeV}/c)^2$ or with both $P_\perp^2$ less than 1.5 $(\mathrm{GeV}/c)^2$ and the visible charged energy less than $0.6E_{\mathrm{beam}}$, where E_{beam} is the electron beam energy. Since particles were often lost down the beam line in these events, we required that the angle between the net momentum of the event and the beam axis, θ_{event}, satisfied $|\cos\theta_{\mathrm{event}}|<0.80$ for events where $P_\perp^2$ was less than 0.5 $(\mathrm{GeV}/c)^2$. Monte Carlo studies indicated that these cuts retained approximately 90% of τ pairs satisfying all other selection criteria and only about 11% of the two-photon events. At this stage of the analysis, two-photon events constituted approximately 1% of the sample.

Like two-photon events, beam-gas events tended to be boosted along the beam direction, and the requirements on the visible charged energy (see Fig. 1), $P_\perp^2$ and $\cos\theta_{\mathrm{event}}$ suppressed these sources of background as well as the two-photon events. From studies of events whose vertex lay more than 5 cm from the nominal collision point along the beam axis, we estimated that 12 beam-gas events remained in the data sample at this stage of the analysis.

The remaining background to the τ pairs consisted primarily of $e^+e^-\to q\bar{q}$ events. It was suppressed by requiring that the 3-prong side of the event be kinematically consistent with a τ decay. We required that the invariant mass of the 3-prong "jet" be less than 1.8 GeV/c^2 and that the square of the missing mass recoiling against it in the decay of the τ be greater than zero. We shall refer to events satisfying these criteria as being in the "signal" region. To calculate the missing mass squared, we assumed that the τ was traveling along the direction of the net momentum vector of the three-prong jet with an energy equal to the beam energy. We then boosted the three prongs to the rest frame of the τ, and computed the mass squared recoiling them. In the absence of measurement errors in the charged-particle momentum vectors, this quantity was positive for τ decays. The selection criteria described above eliminated approximately half of the remaining hadronic and two-photon background, but only 2% of the τ's. The final selected data sample consisted of 15 842 events. Table I summarizes the event selection, and gives the number of events passing each selection criterion.

The background level in this final sample was estimated using Monte Carlo–generated hadronic events normalized to the data. The normalization of the Monte Carlo events to the data was determined using events with 3-prong invariant mass greater than 1.8 GeV/c^2 or missing mass squared less than -0.8 GeV$^2/c^4$. We shall refer to events satisfying these criteria as being in the "normalization" region. This procedure is illustrated in Fig. 2. The shapes of the Monte Carlo and data distributions agree well in the region free of τ's as shown in Fig. 3. We stress the point that we used the Monte Carlo events for the shapes of the distributions, but that the normalization which gave the contamination to our sample was derived from the data. This normalization technique was insensitive to possible systematic errors in the

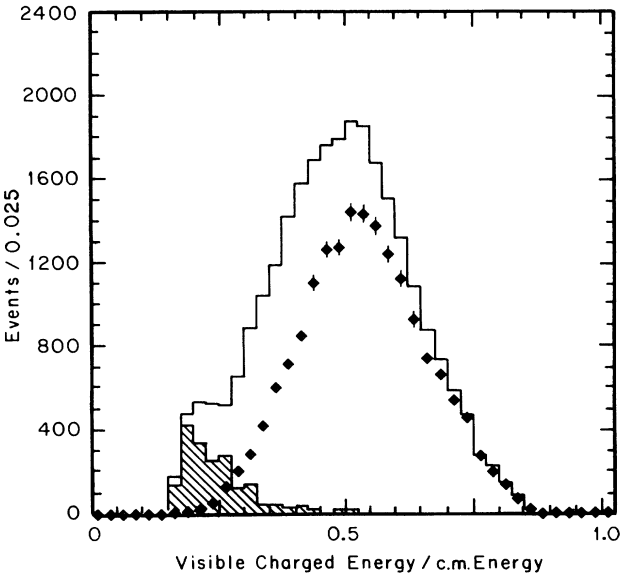

FIG. 1. The distribution of $E_{\mathrm{chg}}/E_{\mathrm{c.m.}}$, where E_{chg} is the sum of the energies of the charged tracks assuming they are pions, and $E_{\mathrm{c.m.}}$ is the center-of-mass energy for the data (open histogram), $e^+e^-\to e^+e^-\gamma\gamma$ Monte Carlo simulation (hatched histogram), and $e^+e^-\to\tau^+\tau^-$ Monte Carlo simulation (diamonds). The two-photon Monte Carlo simulation was normalized to the data in the region with $E_{\mathrm{chg}}/E_{\mathrm{c.m.}}$ less than 0.25, after subtracting τ's and the hadronic and beam-gas backgrounds discussed in the text.

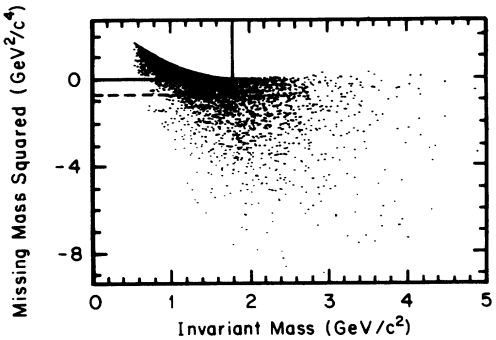

FIG. 2. The missing mass squared versus the 3-prong invariant mass for 1-versus-3 events passing all other selection criteria. The τ signal lies within the solid rectangle; the region outside the dashed rectangle (missing mass squared <-0.8 GeV$^2/c^4$ or 3-prong mass >1.8 GeV/c^2) was used to normalize the Monte Carlo simulation to the data.

TABLE I. Event selection.

Criterion	Events surviving	$\epsilon_{MC}^{1\nu 3}$	$\frac{\epsilon^{1\nu 3}}{\epsilon^{e\nu 3}}$
4 tracks from origin	202 318	0.537	0.983
1-versus-3 topology in fiducial	42 106	0.498	1.020
3-track trigger	39 165	0.893	1.005
No K,μ,e in 3-prong	32 259	0.937	1.000
No photon conversions	30 762	0.961	1.001
$0.7 < p_{1-\text{prong}} < 4.0$ GeV/c	22 648	0.771	0.949
Two-photon cuts	18 574	0.908	1.004
Kinematically consistent with tau	15 842	0.977	0.998
Identified electron 1-prong	2 960		

absolute normalization of the Monte Carlo events. It also accounted for the small two-photon contribution to the background in the same subtraction, since the Monte Carlo simulation indicated that the ratio of the numbers of events in the signal and normalization regions was comparable for two-photon and $q\bar{q}$ events. With this technique, we found that the background fraction in the 1-versus-3 τ sample was 15.8±0.7(stat)%.

The systematic error on the background measurement depended on the accuracy with which the Monte Carlo simulation reproduced the true background distributions. This was estimated from the comparison of the data and Monte Carlo simulation in other similar event samples. The first test used "2-versus-2" events. These were four-track events in which no track satisfied the 1-prong isolation cut. Using the τ Monte Carlo simulation normalized to the 1-versus-3 data sample, we estimated that τ's accounted for approximately 29% of the events in the signal region of this sample. After subtracting this τ contribution, the missing-mass-squared spectrum (calculated using three of the four tracks in the event) was reasonably well reproduced by 2-versus-2 events from the $q\bar{q}$ Monte Carlo simulation, as shown in Fig. 4. The tails of the generated spectrum were normalized to the data following the same procedure used to determine the background fraction in the 1-versus-3 sample. We defined the quantity

$$p = \frac{(N_{\text{signal}}/N_{\text{norm}})_{\text{data}}}{(N_{\text{signal}}/N_{\text{norm}})_{\text{MC}}},$$

where N_{signal} is the number of events in the signal region and N_{norm} is the number of events in the normalization region. The quantity p was then a figure of merit on how well the Monte Carlo simulation predicted the number of events in the signal region from the number of events in

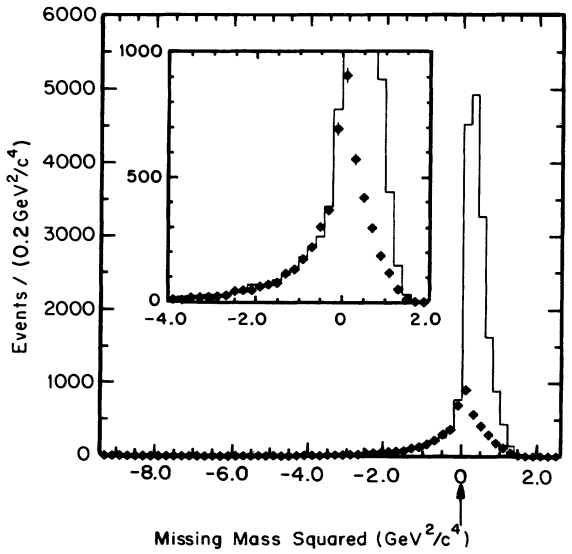

FIG. 3. The missing-mass-squared distribution of 1-versus-3 events from data (histogram) with the $q\bar{q}$ Monte Carlo simulation (diamonds) superimposed. The arrow indicates the position of the cut that defines the signal region. The inset shows a magnification of the region between −4.0 and 2.0 in missing mass squared.

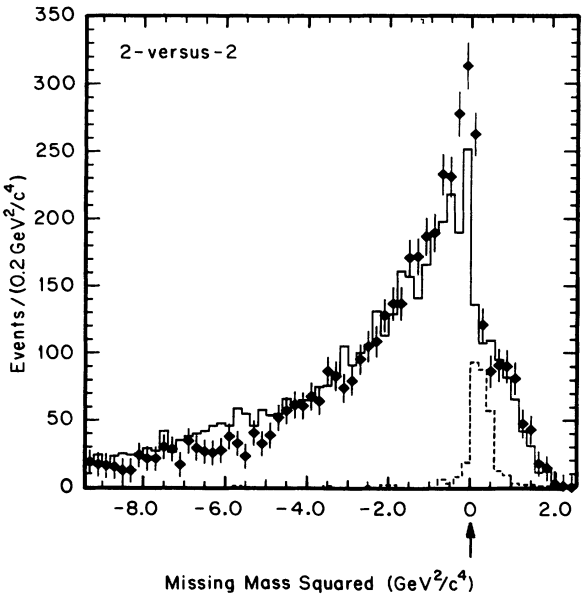

FIG. 4. The missing-mass-squared distribution of 2-versus-2 events from the data (histogram) with the $q\bar{q}$ Monte Carlo simulation (diamonds) superimposed. The 29% contribution to the data from true τ decays, determined by the Monte Carlo simulation, is indicated by the dashed histogram and has been subtracted from the data. The arrow indicates the cut that defines the signal region.

the normalization region. For the 2-versus-2 data sample, $p_{2v2}=0.91\pm0.06$(stat).

A second check of the Monte Carlo simulation of the $q\bar{q}$ distributions used a sample of "2-versus-3" events selected by a procedure similar to that for the 1-versus-3 sample. We required a five track event with two tracks whose total momentum was separated by at least 90° from the remaining three tracks. The τ Monte Carlo simulation predicted the number of true τ events in this sample; they accounted for 5% of the observed events. After subtracting this 5% τ contamination, and following the same procedure of normalizing the Monte Carlo simulation to the data in the normalization region, we found $p_{2v3}=0.97\pm0.03$(stat). The missing-mass-squared spectrum for these events is shown in Fig. 5.

Finally, we carried out the above procedure using a sample of "3-versus-3" events. We required six track events, with three tracks in each hemisphere. We eliminated τ background to this sample by requiring that one of the 3-prong jets, chosen at random, have an invariant mass greater than 1.8 GeV/c^2 and studied the distributions of the other jet. After normalizing the Monte Carlo simulation to the data following the same procedure, we found $p_{3v3}=0.95\pm0.006$(stat). The missing-mass-squared spectrum for these events is shown in Fig. 6.

The average of the results of these three studies p_{2v2}, p_{2v3}, and p_{3v3} was 0.95 ± 0.03(stat). We took this to be the value of p_{1v3} and scaled number of background events by that factor. This reduced the background to the 1-versus-3 data from 15.8% to 15.0 ± 0.7(stat)%.

The procedure just described assumed that inaccuracies in the Monte Carlo simulation of the 1-versus-3 distributions would affect the simulations of the 2-versus-2, 2-versus-3, and 3-versus-3 distributions as well. To test this assumption, we generated Monte Carlo samples using a variety of generation parameters and fragmentation

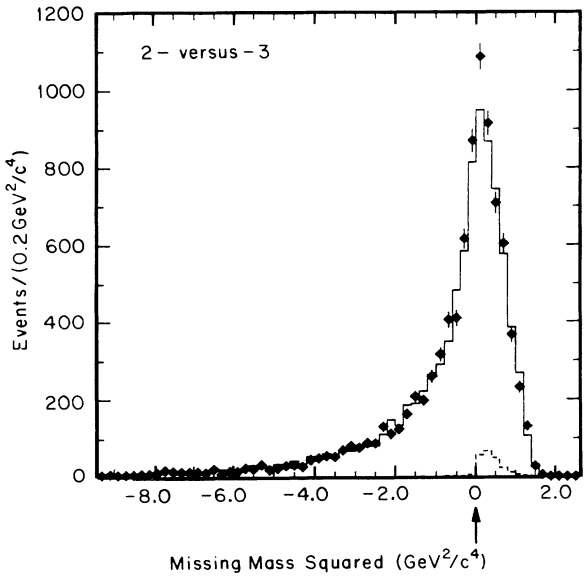

FIG. 5. The missing-mass-squared distribution of 2-versus-3 events in the data (histogram) with the $q\bar{q}$ Monte Carlo simulation (diamonds) superimposed. The 5% contribution to the data from true τ decays, determined by the Monte Carlo simulation, is indicated by the dashed histogram and has been subtracted from the data. The arrow indicates the cut that defines the signal region.

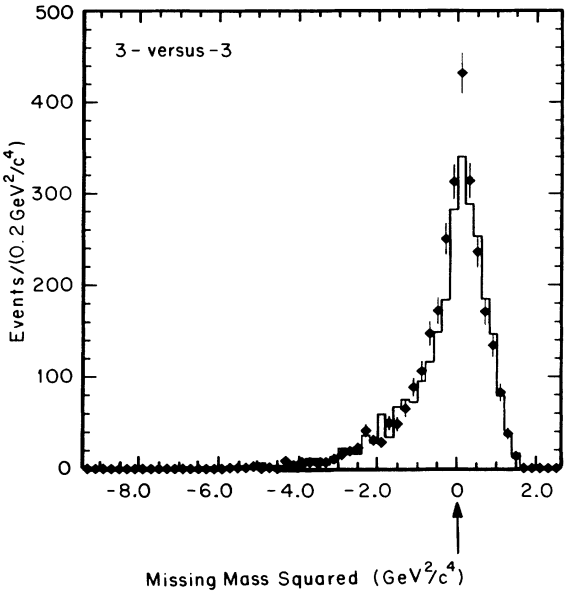

FIG. 6. The missing-mass-squared distribution of 3-versus-3 events in the data (histogram) with the $q\bar{q}$ Monte Carlo simulation (diamonds) superimposed. The arrow indicates the cut that defines the signal region.

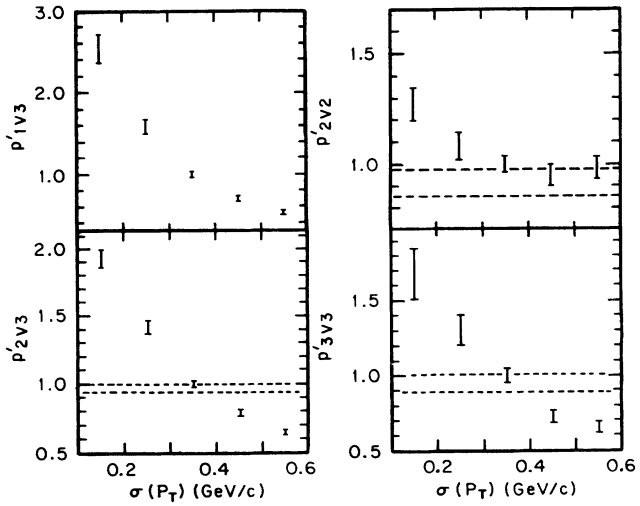

FIG. 7. The dependence of $p'=(N_{\text{signal}}/N_{\text{norm}})^{\text{new}}_{\text{MC}}/(N_{\text{signal}}/N_{\text{norm}})^{\text{std}}_{\text{MC}}$ on the width of the transverse-momentum distribution of particles about the jet axis, $\sigma(P_T)$, with which the Monte Carlo events are generated for the 1-versus-3, 2-versus-2, 2-versus-3, and 3-versus-3 topologies. This is the parameter to which the value of $(N_{\text{signal}}/N_{\text{norm}})_{\text{MC}}$ for the 1-versus-3 sample was most sensitive. The dashed lines indicate the one standard deviation range of each study.

TABLE II. Background summary.

Source	Contribution to 1-versus-3	Contribution to e-versus-3
$e^+e^- \to q\bar{q}$	14.5±0.7%	1.4±0.4%
$e^+e^- \to e^+e^- q\bar{q}$	~0.5%	0.9±0.3%
$e^+e^- \to e^+e^- l^+l^-$	0	<0.2%
Beam-gas	<0.1%	<0.1%
Radiative Bhabha events		<0.1%
Electron misidentification		1.2±0.4(syst)%
Total	15.0±0.7(stat)%	3.5±0.5(stat)%
Systematic uncertainty	±1.6%	±0.6%

models. For each parameter set, we measured the value of $(N_{\text{signal}}/N_{\text{norm}})_{\text{MC}}$ for each of the four topologies and compared it to the corresponding value obtained with our standard Monte Carlo parameters. The ratio of the new to the standard value was then given by

$$p' = \frac{(N_{\text{signal}}/N_{\text{norm}})^{\text{new}}_{\text{MC}}}{(N_{\text{signal}}/N_{\text{norm}})^{\text{std}}_{\text{MC}}} .$$

Figure 7 shows how this quantity changed as a function of the most sensitive parameter, the rms momentum of the generated particles transverse to the jet axis, $\sigma(P_T)$, for each of the topologies that we studied. As shown in the figure, for values of this parameter consistent with the 2-versus-2, 2-versus-3, and 3-versus-3 data the value of p'_{1v3} lies within the range $0.85 < p'_{1v3} < 1.05$. We assigned a systematic uncertainty on p_{1v3} of ±0.10, which was consistent with these studies and covered the statistical ranges of p_{2v2}, p_{2v3}, and p_{3v3}. This uncertainty corresponded to a systematic uncertainty on the hadronic background fraction of ±1.6% corresponding to a relative error on R of ±1.9%. Table II summarizes the backgrounds to the 1-versus-3 sample.

IV. THE ELECTRON-TAGGED SAMPLE

Electrons were identified using the specific ionization of the track in the drift chamber and the dE/dx modules, the pulse height in the time-of-flight counters, the ratio of the energy deposited by the particle in the electromagnetic calorimeter to the particle's momentum, and the spatial distribution of the energy in the calorimeter. The distributions of these variables for electrons and hadrons were determined using Bhabha interactions and events at the $\Upsilon(1S)$, respectively. For each 1-prong track the ratio of electron to hadron likelihoods was determined, and events were tagged as electrons if the log of this ratio was greater than three. The final data sample, after all cuts, contained 2960 identified electrons among the 1-prong candidates.

One-prong τ decays in which a π, K, or μ was mistaken for an electron contributed to this electron tagged sample. To determine the contamination from these events we measured the misidentification probability as a function of momentum for π's, K's, and μ's using samples culled from K_S decays, D decays and $e^+e^- \to \mu^+\mu^-\gamma$ interactions, respectively. These probabilities were then combined using the expected particle abundances in the 1-prong τ decays. This subtraction procedure did not necessarily account for 1-prong τ decays in which an energetic photon from π^0 or η decay overlapped a charged π in the calorimeter. Monte Carlo studies showed that this overlap probability was small, about 0.6%, and comparable for the 1-prong τ decays and for the π's from K_S decays used to determine the misidentification probability; furthermore it affected primarily low momentum $\pi^{\pm}$, for which dE/dx information dominated the electron likelihood. We searched the electron-tagged sample for these overlaps using the distribution of the distance from the shower in the calorimeter to the position of the extrapolated track. This distribution was sharply peaked as expected for true electrons, with no evidence for background. The overall misidentification probability was 0.26±0.09(syst)% per track, and resulted in 35±12(syst) wrongly identified electrons.

Backgrounds specific to the electron sample came from photon conversions, Dalitz decays, radiative Bhabha events, and two-photon interactions with purely leptonic final states. These background events could have passed our selection criteria only if one or more electrons were lost or misidentified. The background due to Dalitz decays was determined from the Monte Carlo simulation to be negligible. Radiative Bhabha and two-photon events to leptonic final states were expected to contribute less than 3 and 6 events, respectively, to the final sample. The background due to beam-gas interactions was determined using events whose origins were displaced along the beam axis, and was approximately 0.8 events.

A significant background to the electron sample was two-photon interactions with hadronic final states. Monte Carlo studies indicated that two processes contributed to this background with roughly equal probability. In one, the electron was the product of the decay of a hadron, while in the other, a hard scatter caused one of the beam electrons to appear in the detector as the 1-prong candidate. Monte Carlo simulation indicated that these processes together contributed 27±8(stat) events. To test our understanding of this background we removed the cuts to suppress the two-photon events. Doing so doubled the number of events in the normalization regions of the electron and the generic 1-versus-3 samples; however, after accounting for the backgrounds, the measured branching ratio changed by less than 0.2% of its value.

The background due to the two-photon process in which one of the beam electrons scattered into the detector could also be determined using the data directly. In these events one final-state particle had to be lost down the beam pipe if the detected particles were to have a net charge of zero. Since the charge of the lost particle was random, events of this topology were equally likely to have a net charge of two as a net charge of zero. When we analyzed events with a net charge of two, we found six that satisfied all selection requirements for the e-versus-3 sample. This number was slightly lower than the Monte Carlo prediction of 18 ± 8 events. The difference between data and Monte Carlo simulation was included in the systematic error below.

The other significant background to the electron sample was from $e^+e^-\rightarrow q\bar{q}$ interactions containing either the semileptonic decay of a charmed quark or a hadron mistaken for an electron. This background was determined from a Monte Carlo simulation using the normalization technique described previously for the generic 1-prong sample, after subtracting the two-photon contribution. It was found to be 40 ± 11(stat) events. The Monte Carlo normalization could also be determined (with a larger systematic uncertainty) from that of the 1-versus-3 sample and the fraction of $q\bar{q}$ Monte Carlo events in which the 1-prong was an electron. This technique yielded 52 ± 2(stat) events, consistent with the results of the other method.

As was the case for the generic 1-versus-3 sample, the systematic uncertainty in the background to the e-versus-3 sample arose from uncertainty in the 3-prong invariant-mass and missing-mass-squared distributions of the background. For the electron-tagged sample, just as for the untagged sample, these distributions were similar for the two-photon and hadronic events, and so the number of background events was insensitive to the fraction of events in the normalization region attributed to each source. Assuming that the events in the normalization region were entirely due to hadronic events or entirely due to two-photon interactions changed the total background level by ±8 events. This variation, combined with the small uncertainty in the contributions of the two-photon processes with purely leptonic final states and radiative Bhabha scattering, and with the uncertainty in the number of falsely identified electrons, give a total systematic uncertainty on the background to the electron-tagged sample of $\pm0.6\%$.

Table II lists the backgrounds to the e-versus-3 sample. After subtracting backgrounds and misidentified hadrons and muons, the number of electrons in the 1-prong sample was 2856 ± 56(stat), where the error includes the statistical contributions from the subtractions.

V. DETECTION EFFICIENCY

In order to determine the value of R we needed to know the ratio of the 1-versus-3 to e-versus-3 event detection efficiencies. This ratio could be expressed as

$$\frac{\epsilon^{1v3}}{\epsilon^{ev3}}=\frac{\epsilon^{1v3}_{\rm MC}}{\epsilon^{ev3}_{\rm MC}\times\epsilon_{\rm ID}},$$

where $\epsilon^{1v3}_{\rm MC}$ and $\epsilon^{ev3}_{\rm MC}$ include the effects of triggering, track reconstruction, and event selection, and $\epsilon_{\rm ID}$ is the efficiency for correctly identifying a track as an electron. Using the Monte Carlo simulation of τ decays in the CLEO I detector, we found $\epsilon^{1v3}_{\rm MC}=0.147\pm0.001$(stat) and $\epsilon^{ev3}_{\rm MC}=0.153\pm0.001$(stat). The efficiencies of the individual selection criteria for the 1-versus-3 decays appear in Table I.

Differences between $\epsilon^{1v3}_{\rm MC}$ and $\epsilon^{ev3}_{\rm MC}$ arose from several sources. About 2% of 1-versus-3 decays had more than four tracks because of a K_S or Dalitz decay. (We have followed the convention that charged pions from K_S decay contribute to the count of the number of prongs; electrons from Dalitz decay do not.) The efficiency of the geometric selection criteria depended on the angular distribution of the 1-prong track with respect to the 3-prong jet, and therefore differed slightly for e-versus-3 and 1-versus-3 events. The momentum spectrum of generic 1-prongs was softer than that of the electrons (the difference in their mean momenta was 0.05 GeV/c), leading to a 5% difference in the fraction of events surviving the momentum cut [10]. We studied the ratio of $\epsilon^{1v3}_{\rm MC}$ to $\epsilon^{ev3}_{\rm MC}$ as we varied the cuts used to purify the sample and assigned a systematic uncertainty of $\pm1.0\%$ on the result based on the study.

Another source of the difference in the detection efficiencies was the CLEO I trigger requirement. Here, potential biases arose from the difference in the average energy deposited in the calorimeter for the 1-versus-3 and e-versus-3 decays and from the presence of extra photons in the generic 1-prong decays which could convert and fire the time-of-flight counters. While τ decays could satisfy any one of several triggers, we only accepted events satisfying the trigger that was least sensitive to these effects. This trigger required three tracks and hits in time-of-flight counters in nonadjacent octants of the detector. The efficiency of this trigger was about 89% for events passing all other selection criteria, and was nearly identical for the e-versus-3 and 1-versus-3 samples. We checked the trigger simulation by comparing the matrix of trigger probabilities of the data with that predicted by the Monte Carlo simulation. This study led to assignment of a systematic uncertainty of $\pm1.5\%$ due to simulation of the trigger. The efficiency ratio for 1-versus-3 and for e-versus-3 events is summarized in the last column of Table I.

The efficiency for identifying an electron within the fiducial volume, $\epsilon_{\rm ID}$, was determined using radiative Bhabha events. It is shown as a function of momentum in Fig. 8. The average efficiency was 90.9 ± 0.6(stat)%. Figure 9 shows the momentum spectrum for electrons in our data after background subtraction together with the spectrum predicted by the Monte Carlo including electron identification efficiency.

Errors in the electron identification could arise from biases in the selection of the radiative Bhabha events used to measure the efficiency. The Bhabha events were selected if they had two tracks plus one additional shower in the calorimeter which together were kinematically consistent with radiative Bhabha scattering. The resulting

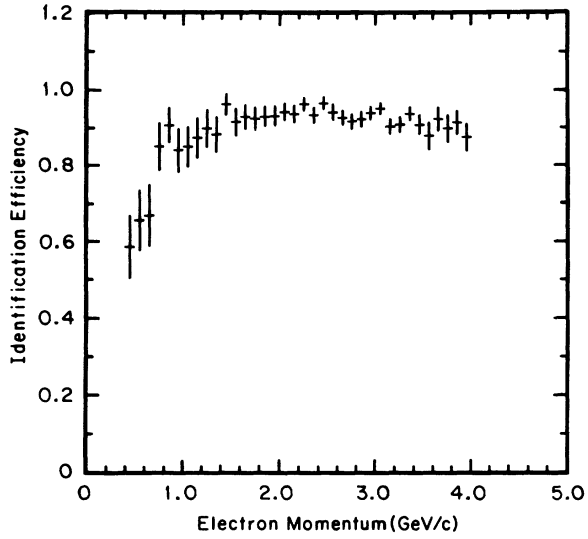

FIG. 8. The electron finding efficiency as a function of momentum.

efficiencies were found to be insensitive to the details of the selection criteria, such as the maximum allowed χ^2 defining kinematic consistency or the minimum allowed separation of the showers in the calorimeter. A small dependence on the angle of the track with respect to the beam axis (θ) was observed and corrected for. The electron-identification efficiencies also could be checked independently using the τ sample itself. To do this, we selected a sample of electrons from the 1-versus-3 τ decays using a subset of the variables contributing to the likelihood ratio. We then used these electrons to calculate the identification efficiency for the remainder of the variables contributing to the likelihood ratio; after correcting for nonelectrons in the sample, this efficiency could be compared with that obtained from Bhabha events for the same reduced set of variables. This study yielded the same efficiencies as the Bhabha study within $1.8\pm2.6\%$.

The electron identification efficiency could have been underestimated if there were nonelectrons present in the Bhabha sample. To search for background, all events flagged as possible background events were scanned by hand, and a small number of events, corresponding to 1% of the full Bhabha sample, was discarded.

As a final study of the electron identification efficiency, we varied the likelihood cut used to identify electrons, and after accounting for the change in the misidentification probability, we saw negligible change in the result. Based on all these studies, we assigned a systematic uncertainty on the identification efficiency of $\pm1\%$.

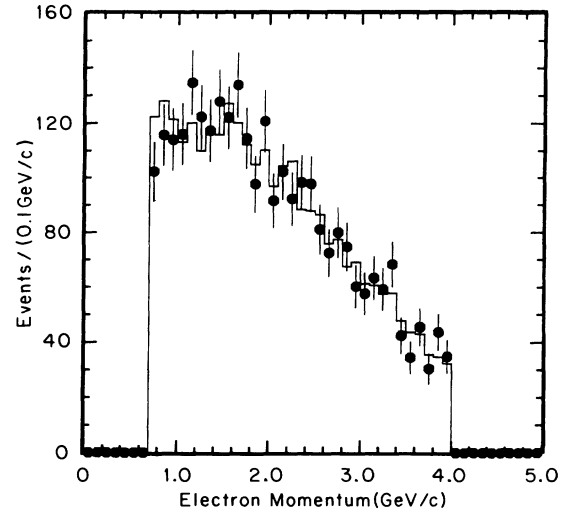

FIG. 9. The momentum spectra of electrons in the data (points) and Monte Carlo simulation (histogram) normalized between 0.7 and 4.0 GeV/c. Hadronic background and the contamination by non-electrons have been subtracted from the data; the Monte Carlo simulation has been corrected for the electron identification efficiency.

VI. DETERMINATION OF THE BRANCHING RATIO

We now turn to the extraction of the electronic branching fraction from the data. In general, the number of 1-versus-3 decays produced, N_{1v3}, is given by $N_{1v3}=2NB_1B_3$, where N is the total number of τ pairs produced and B_1 and B_3 are the τ topological 1-prong and 3-prong branching fractions. Similarly, the total number of e-versus-3 decays produced, N_{ev3}, is given by $N_{ev3}=2NB_eB_3$, where B_e is the electronic branching fraction. Together these expressions yield $B_e/B_1=N_{ev3}/N_{1v3}$. We note that in this ratio the total number of τ pairs produced, N, and the 3-prong branching fraction B_3 cancel. We calculated the values of N_{1v3} and N_{ev3} for our data sample using $N_{jv3}=a_jN_{jv3}^{\rm gen}$, where $N_{jv3}^{\rm gen}$ was the number of j-versus-3 decays generated in the Monte Carlo simulation and a_j was the ratio of luminosities of the data and Monte Carlo samples. The values of a_j were determined by minimizing χ^2 given by

$$(\chi^2)^j=\sum_i\frac{[N_{jv3}^{\rm obs}(\text{data})-a_jN_{jv3}^{\rm obs}(\text{MC})]_i^2}{\sigma_i^2},$$

where $N_{jv3}^{\rm obs}$(data) was the number of events in the background-subtracted data sample and $N_{jv3}^{\rm obs}$(MC) was the number of accepted Monte Carlo events, and was related to the efficiencies via $N_{jv3}^{\rm obs}(\text{MC})=\epsilon^{jv3}N_{jv3}^{\rm gen}$. The error in each bin, σ_i, included the contributions from the background-subtraction and electron identification efficiency, as well as the statistical errors on the data and Monte Carlo samples. The sum was over 100-MeV/c momentum bins from 0.7 to 4.0 GeV/c [11]. Combining the above expressions for the two modes as outlined above, we found

$$R=B_e/B_1=0.2231\pm0.0044(\text{stat})\pm0.0073(\text{syst}),$$

where the first error is from the statistics of the data and the second is the systematic error and included the sta-

TABLE III. Contributions to the systematic error in the measurement of R, excluding statistical contributions from the Monte Carlo simulation and background subtractions.

Source	σ_R/R (%)
Background subtraction	
1-versus-3	1.9
e-versus-3	0.6
Electron ID efficiency	1.0
$\epsilon_{MC}^{1\nu 3}/\epsilon_{MC}^{e\nu 3}$	
Sensitivity to cuts	1.0
Trigger simulation	1.5
1-prong branching ratios	0.3
3-prong branching ratios	0.6
Total	2.9

tistical error on the efficiency and backgrounds (± 0.0036). The dominant systematic errors are summarized in Table III.

Several further checks for systematic effects were performed. First, we removed the kinematic cuts which normally suppress the $q\bar{q}$ background and recalculated R; the result was consistent with the reported value although the background in the 1-prong sample was higher by a factor of 2. Varying the τ 3-prong branching fractions by one standard deviation [2] changed the ratio of generic to electron-tagged detection efficiencies by ± 0.6(syst)%. The sensitivity to variations in the 1-prong branching fractions was ± 0.3(syst)%. We also searched for systematic effects on the result by measuring the branching ratio as a function of center-of-mass energy, time, and the momentum and charge of the 1-prong track. No deviations were observed outside of the statistical errors.

To calculate the electronic branching fraction, we used the value [2] $B_1 = 0.861 \pm 0.003$. The result is

TABLE IV. Partial summary of experimental values of $B(\tau \to e\bar{\nu}_e\nu_\tau)$.

Experiment	B_e
DELCO [12] 1978	0.160 ± 0.013
Mark III [13] 1985	$0.182 \pm 0.007 \pm 0.005$
MAC [14] 1985	$0.180 \pm 0.009 \pm 0.006$
JADE [15] 1986	$0.170 \pm 0.007 \pm 0.009$
Mark II [16] 1987	$0.191 \pm 0.008 \pm 0.011$
TPC [17] 1987	$0.184 \pm 0.012 \pm 0.010$
CELLO [18] 1990	0.186 ± 0.009
OPAL [19] 1991	$0.174 \pm 0.005 \pm 0.004$
This work	$0.192 \pm 0.004 \pm 0.006$

$$B_e = 0.192 \pm 0.004(\text{stat}) \pm 0.006(\text{syst}) .$$

Table IV compares this result with some of the previous measurements of B_e. This result is 1.8 standard deviations larger than the current world average [2] of $B_e = 0.177 \pm 0.004$, and is consistent with the experimental value of the τ lifetime.

ACKNOWLEDGMENTS

We gratefully acknowledge the effort of the CESR staff in providing us with excellent luminosity and running conditions. P.S.D. thanks the PYI program of the NSF, K.H. thanks the Alexander von Humboldt Stiftung Foundation, G.E. thanks the Heisenberg Foundation, and R.P. and P.R. thank the A.P. Sloan Foundation for support. This work was supported by the National Science Foundation and the U.S. Department of Energy. The supercomputing resources of the Cornell Theory Center were used in this research.

[1] Y. S. Tsai, Phys. Rev. D **4**, 2821 (1971).

[2] Particle Data Group, J. J. Hernández *et al.*, Phys. Lett. B **239**, 1 (1990).

[3] Toichiro Kinoshita and Alberto Sirlin, Phys. Rev. **113**, 1652 (1958).

[4] D. Andrews *et al.*, Nucl. Instrum. Methods **211**, 47 (1983); D. G. Cassel *et al.*, *ibid.* **A252**, 325 (1986).

[5] R. D. Field and S. Wolfram, Nucl. Phys. **B213**, 65 (1983).

[6] T. Sjostrand, Comput. Phys. Commun. **27**, 243 (1982); **28**, 227 (1983).

[7] T. Sjostrand, Comput. Phys. Commun. **39**, 347 (1986); M. Bengtsson and T. Sjostrand, Nucl. Phys. **B283**, 810 (1987).

[8] S. Jadach, J. H. Kuhn, and Z. Was, Report No. CERN-TH-5856/90 (unpublished); S. Jadach and Z. Was, Comput. Phys. Commun. **36**, 191 (1985).

[9] J. R. Smith, Ph.D. thesis, University of California at Davis, 1982.

[10] In the Monte Carlo simulation, $\tau \to e\nu_\tau\bar{\nu}_e$ decays occurred via normal $V-A$ interactions with the spectrum softened slightly because of internal bremsstrahlung [Ref. [3]; David Atwood and William Marciano, Phys. Rev. D **41**, 1736 (1990)] and energy loss in the detector. We have studied sensitivity of the result to the value of the Michel parameter ρ, which describes the relative $V-A$ and $V+A$ contributions to the τ-decay vertex. A pure $V-A$ interaction corresponds to $\rho = 0.75$, while pure $V+A$ corresponds to $\rho = 0$. A change of 0.05 in the Michel parameter from the value 0.75 would change our value of R by less than 0.25% of itself.

[11] We note that if we did not break our data into 100-MeV momentum bins, the calculation of B_e/B_1 would reduce to

$$B_e/B_1 = \frac{N_{e\nu 3}^{\text{obs}}(\text{data}) N_{e\nu 3}^{\text{gen}}/N_{e\nu 3}^{\text{obs}}(\text{MC})}{N_{1\nu 3}^{\text{obs}}(\text{data}) N_{1\nu 3}^{\text{gen}}/N_{1\nu 3}^{\text{obs}}(\text{MC})} .$$

By minimizing the χ^2 in the fashion described, we correctly weighted the contributions to the error in each momentum bin from electron identification efficiency, electron misidentification, and background subtractions, in addition to the statistical errors on the data and Monte Carlo samples.

[12] DELCO Collaboration, W. Bacino *et al.*, Phys. Rev. Lett. **41**, 13 (1978).

[13] Mark III Collaboration, R. M. Baltrusaitis *et al.*, Phys. Rev. Lett. **55**, 1845 (1985).

[14] MAC Collaboration, W. W. Ash *et al.*, Phys. Rev. Lett. **55**, 2118 (1985).

[15] JADE Collaboration, W. Bartel *et al.*, Phys. Lett. B **182**, 216 (1986).
[16] Mark II Collaboration, P. Burchat *et al.*, Phys. Rev. D **35**, 27 (1987).
[17] TPC Collaboration, H. Aihara *et al.*, Phys. Rev. D **35**, 1553 (1987).
[18] CELLO Collaboration, H. J. Behrend *et al.*, Z. Phys. C **46**, 537 (1990).
[19] OPAL Collaboration, G. Alexander *et al.*, Phys. Lett. B **266**, 201 (1991). This result was published after the compilation by the Particle Data Group and is not included in the world average.